Seasonal variations in GPS time series from the Nepal Himalaya : Evaluation of atmospheric effects and land-water storage variations

Pierre Bettinelli[1]; Mireille Flouzat[1]; Jean-Philippe Avouac[2]; Thierry Héritier[1]; Umesh Gautam[3]

[1]Commissariat à l'Energie Atomique, Laboratoire de Détection et de Géophysique, 91680 Bruyères-Le-Châtel, France, E-mail: mireille.flouzat@cea.fr

[2]Tectonics Observatory, California Institute of Technology, Pasadena, CA91125, USA, E-mail: avouac@gps.caltech.edu

[3]Department of Mines and Geology, National Seismological Center, Lainchaur, Kathmandu, Nepal, Email: nscdmg@mos.com.np

Abstract

Geodetic times series from continuous GPS (CGPS) stations across the Himalaya of central Nepal show strong seasonal fluctuations observed on the horizontal and vertical components. Because the fluctuations determined at the different stations have similar phase but different amplitudes, these data suggest that the secular shortening across the range is modulated by a seasonal strain. Given the geographic and climatic setting the potential that this observation be biased by tropospheric effects.

Erroneous estimate of the tropospheric delays can in principle generate systematic errors of positioning. This can arise from misestimate of zenithal delays, or, from oversimplification of the tropospheric effects. In our study, the processing assumes a 1-D tropospheric model (only vertical variations are allowed), while it is clear that there must be horizontal gradients in the Himalayan context. In this setting, a latitudinal gradient of tropospheric effect is expected and may well vary seasonally.

In the following we first check that the zenithal delays determined from the GPS data are consistent with in situ meteorological data. The principle of the analysis is that systematic errors in the estimate of zenithal delays should induce positioning artefacts correlated and in-phase with the zenithal delays themselves. In addition, the bias would be expected to be largest on the vertical components although this latter also poorly resolved due to satellites sky distribution (in half a sphere), but could contribute to some systematic errors of horizontal positioning. Next, we evaluate the N-S horizontal gradient of tropospheric delays and its temporal variation. Such variations could indeed generate systematic errors. If so, the effect should be dominant on horizontal positions. Again, a simple test of this potential bias consists in estimating the phase shift between the two time series. Because all the time series involved in this analysis are close to being harmonic functions with an annual period, phases are estimated from least squares adjustment of sine functions.

The zenithal tropospheric delays resulting from the Bernese inversion are shown in Fig. 5. As expected from the geographic setting both their absolute value and the amplitude of the seasonal variations decrease northwards. We have compared qualitatively these delays with those estimated from the in situ meteorological measurements of pressure, temperature and relative humidity . We used data from stations close to SIMR, NAGA and DAMA. There is no meteorological station near our northernmost GPS station (GUMBA).

The tropospheric model used during the GPS Bernese V4.2 processing is the one from [Saastamoinen (1974), Eq 2]. The water vapor partial pressure is deduced from the value of the water vapor saturating pressure, which itself is related to the temperature (Eq. 3 and 4).

This model was also used here to calculate the range of tropospheric delays expected using the daily maximum and minimum pressure, temperature and percentages of humidity. For the three stations NAGA, SIMR and DAMAN, the zenithal delays computed from the GPS data and from the meteorological data agree remarkably well, both in terms of the phase and amplitude of the signal (Fig. 6). Tropospheric delay peaks in the summer are due to a dramatic increase in the percentage of moisture during the monsoon (Figs 5 and 6). This shows that despite the complex meteorological setting the variations of the meteorological data are consistent with those of tropospheric delays inverted form the GPS stations. However, we cannot exclude that, due to potential limitations of the Saastamoinen model, some errors in second order could remain in the corrections. In that case, some correlations should be found between the temporal variations and the inverted zenithal delays.

The comparison of the detrended horizontal component and of the tropospheric delays shows that they are clearly not in phase (Fig. 7). All time series show a strong seasonality, although with somewhat different time structure, and can be fitted well with harmonic functions assuming an annual period (Fig. 7, continuous lines). The phase, expressed in days, of each sine function is indicated on each plot and is reported in Table 3. The phase shift between the horizontal seasonal displacements and the tropospheric delays is about 4 months. This phase shift is clear indication that the seasonal variation in the GPS horizontal time series is probably not due to a mismodelling of the tropospheric zenithal delays. Tropospheric artefacts can not be responsible for the observed seasonality also because, contrary to what is observed, the seasonal variations in the vertical components should then be in phase with the seasonal horizontal displacements and about one order of magnitude larger. The phase-shift between the vertical data and the tropospheric delays is less obvious at station SIMR. This smaller phase-shift might reflect somewhat stronger tropospheric bias at this station which lies in the foreland. Also, we note that the vertical component varies more in phase with the tropospheric delays, than the horizontal component. This is consistent with potential bias on the vertical position, although the temporal variations of the vertical component of the stations of DAMA, NAGA and GUMB might be induced by local loading effects which might not show on the horizontal components.

Although only a 1-D vertical troposphere gradient is used in our processing it is possible to estimate the latidudinal gradient at any time by from the variation of zenithal delays across the range (Fig. 8). Due to the different amplitude of the seasonal variation of zenithal delays at the various station the gradient does vary significantly over the year and this variation is in phase with the zenithal delays themselves (Fig. 9), and out of phase by about 4 month with respect to the variation of the horizontal positions (Fig. 10). It is therefore highly improbable that the variation of horizontal positions be due to this effect. To investigate further that possible bias we have compared the results of our processing of the time series from GUMB, with the results from a processing carried out by with GIPSY at the Jet Propulsion Laboratory, using the Precise Point Positioning processing [Zumberge et al., 1997]. The processing with GIPSY was done allowing one vertical and one horizontal tropospheric gradient [Bar-Sever et al., 1998]. The two time series are extremely close with equivalent seasonal variation with a rms between the two time series equal to 9mm (Fig. 11). It thus appears that the influence of horizontal tropospheric gradient is negligible. This study adds support to the view that the seasonal strain in the Himalayan is real and probably is driven by surface load variations (Fig12&13).

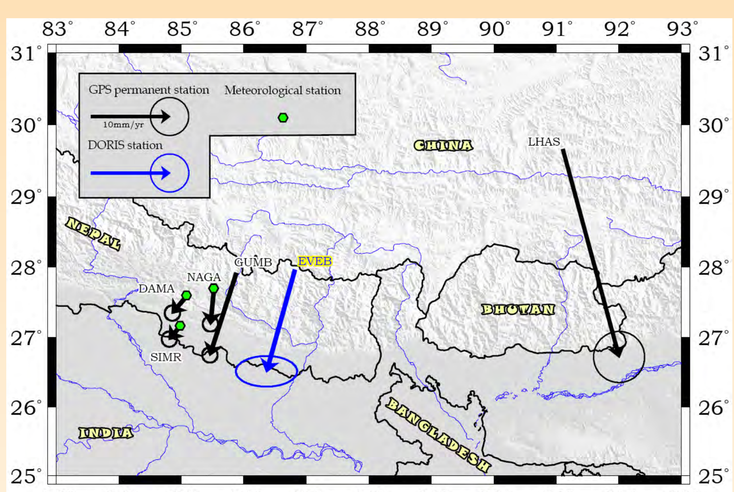

Fig. 1: Location of the CGPS stations and meteorological stations analysed in this study. Black vectors show secular geodetic velocities relative to stable India determined by Bettinelli et al., (2006). The secular velocity at the DORIS station near Mount Everest (blue vector) and the LHAS station are also shown for comparison.

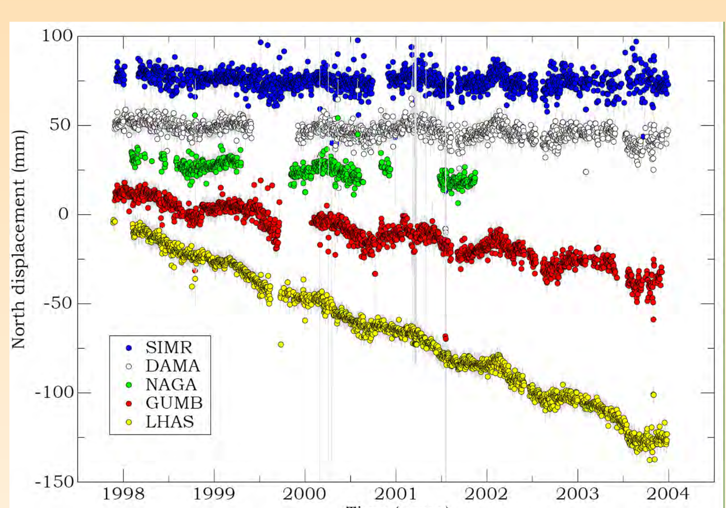

Fig. 2: North component time series of the 5 CGPS stations discussed in this study. Positions were determined relative to the Indian plate as defined by (Bettinelli et al., 2006). Error bars correspond to 1-σ uncertainties. See Fig. 1 for location of stations.

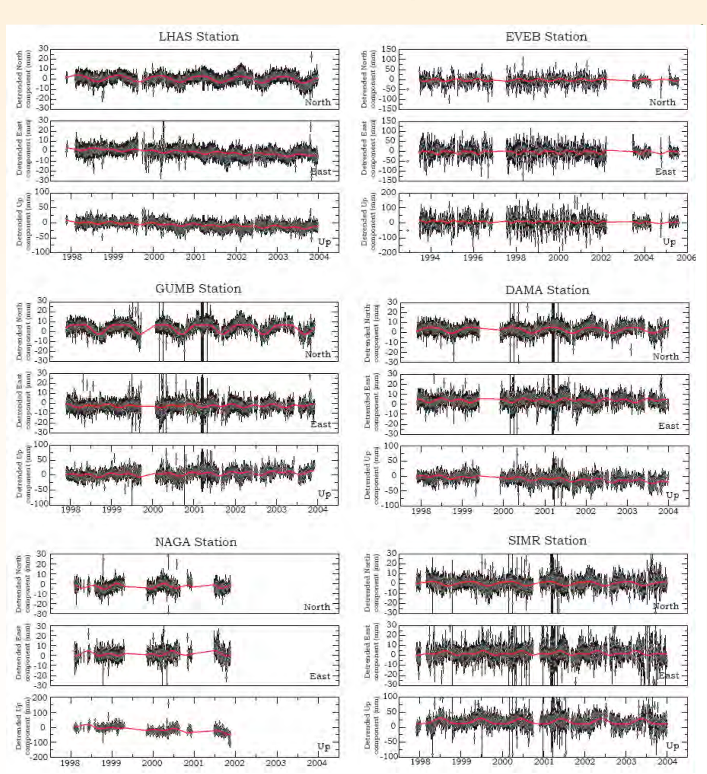

Fig. 3: Observed NS, EW and vertical daily positions at stations SIMR, DAMA, GUMB, NAGA and LHAS (EVEB is expressed in weekly positions). The time series were detrended by removing the secular motion of each station as determined from least-squares adjustment of the times series with equation (1).

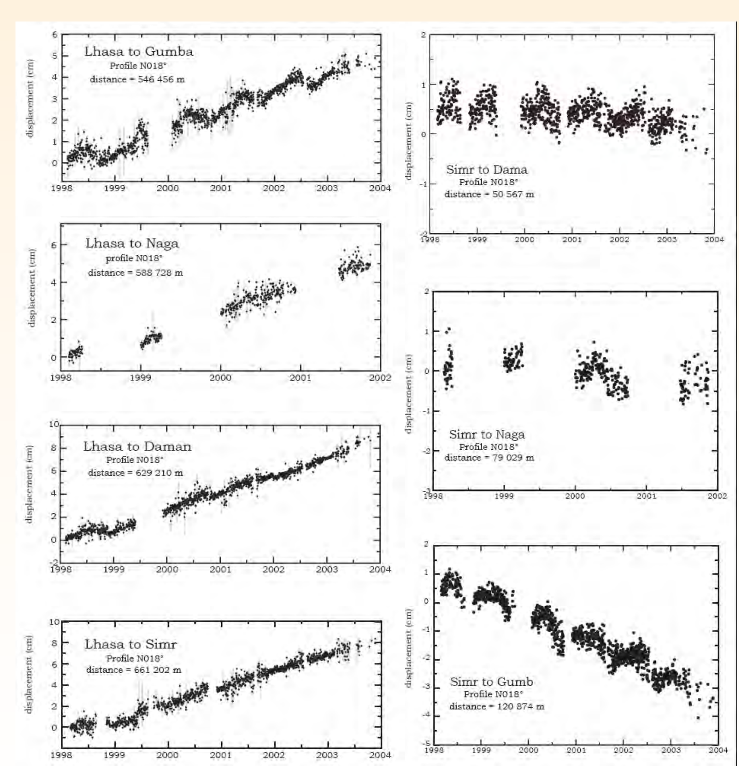

Fig. 4: Time series showing the baselines length changes projected onto the N018° direction (approximate direction of convergence across the Himalaya of central Nepal) computed relative to LHASA (left) and SIMR (right).

IGS station	DOMES number	Longitude	Latitude
BAHR	24901M002	050,6080	026,2090
BAKO	23101M002	106,8490	-006,4910
BJFS	21601M001	115,8920	039,6090
DGAR	30802M001	072,3700	-007,2700
IISC	22306M002	077,5700	013,0210
IRKT	12313M001	104,3160	052,2190
KIT3	12334M001	066,8850	039,1350
KSTU	12349M002	092,7940	055,9930
KUNM	21609M001	102,7970	025,0300
LHAS	21613M001	091,1040	029,6570
MALD	22901S001	073,5260	004,1890
NTUS	22601M001	103,6800	001,3460
POL2	12348M001	074,6940	042,6800
SEY1	39801M001	055,4800	-004,6740
SHAO	21605M002	121,2000	031,1000
TAIW	23601M001	121,5370	025,0210
URUM	21612M001	087,6010	043,8080
WUHN	21602M001	114,3570	030,5310
XIAN	21614M001	109,2210	034,3690

Table 1: List and location of IGS stations taken into account in the processing. Also reported is the DOMES number (International IGS numbering system) of the stations.

		coefficients						
		b	c	d	T	φ1	φ2	χ2
LHAS	North	12.8±1	-1.45±0.2	2.87±0.1	365±0.007	347±2	76±3	10.4
	East	45.3±1	-0.83±0.1	0.33±0.3	364±0.01	165±3	75±4	17.4
	Up	7.6±3	-1.10±0.1	-1.84±0.05	364±0.001	295±2	14±5	99.9
EVEB	North	23.5±0.6	5.75±1.6	-2.17±3.3	355±0.02	341±6	70±6	483.3
	East	36.5±1.2	-6.63±0.3	2.82±0.7	346±0.003	159±8	69±7	1638.4
	Up	-6.1±4.1	1.95±0.5	4.26±0.3	365±0.004	320±2	49±8	650.4
GUMB	North	25.74±0.3	-4.51±0.2	-0.92±0.6	364±0.004	358±2	87±5	16.5
	East	36.15±0.3	-0.66±0.2	-0.61±0.2	365±0.008	178±3	88±6	35.2
	Up	4,4±1	4.21±0.04	-0.07±0.1	365±0.0007	301±5	30±3	218.2
NAGA	North	30.13±0.3	0.41±0.7	0.89±0.4	410±0.03	354±3	83±5	13.6
	East	35.08±0.3	-1.48±1.2	-0.26±4.4	374±0.1	180±2	90±6	43.4
	Up	0,7±1	6.25±1.2	3.92±1.6	383±0.008	202±4	111±5	363.3
DAMA	North	31.90±0.3	2.01±0.6	-2.21±0.5	355±0.007	343±4	72±4	18.6
	East	37.08±0.3	-0.09±0.2	-1.04±0.05	365±0.007	163±6	73±5	39.2
	Up	0,6±1	3.02±0.2	-2.37±0.3	355±0.003	355±4	84±5	223.9
SIMR	North	32.75±0.3	1.24±17.3	-1.79±9.2	346±0.2	335±2	64±4	34.8
	East	37.88±0.3	-1.35±0.2	-0.65±0.4	337±0.007	155±6	65±4	107.1
	Up	0,3±1	-7.65±0.8	4.54±2	355±0.007	101±2	10±2	415.5

Table 2: Coefficients of Eq. 1 used to fit the geodetic time-series with account for seasonal variations. Coefficients T correspond to the period expressed, respectively in days. Coefficients b correspond the velocity in mm.yr-1. Coefficients c and d correspond respectively to the amplitudes of the annual and semi-annual periodic variations.

	coefficients					
	c	d	T	φ1	φ2	χ2
Tropo. Delay LHAS	-0,05 ± 0,9	0,004 ± 0,2	363	119 ± 2	29 ± 3	0,015
Tropo. Delay GUMB	-0,04 ± 2,3	0,01 ± 0,05	366	118 ± 5	39 ± 3	0,0009
Tropo. Delay NAGA	-0,014 ± 1,6	-0,008 ± 0,8	364	120 ± 4	32 ± 5	0,0018
Tropo. Delay DAMA	-0,09 ± 0,5	0,004 ± 0,2	362	120 ± 4	32 ± 3	0,002
Tropo. Delay SIMR	-0,05 ± 3,1	0,02 ± 1,5	360	125 ± 3	42 ± 5	0,038
Hori. Tropo. gradient x1000	0,49 ± 11,8	0,15 ± 6,9	365	119 ± 5	30 ± 5	0,002

Table 3: Coefficients of Eq. 1 used to fit the tropospheric delay time-series. Coefficients T and φ correspond respectively to the period and the phase, expressed in days. Coefficients c and d correspond respectively to the amplitudes of the annual and semi-annual periodic variations.

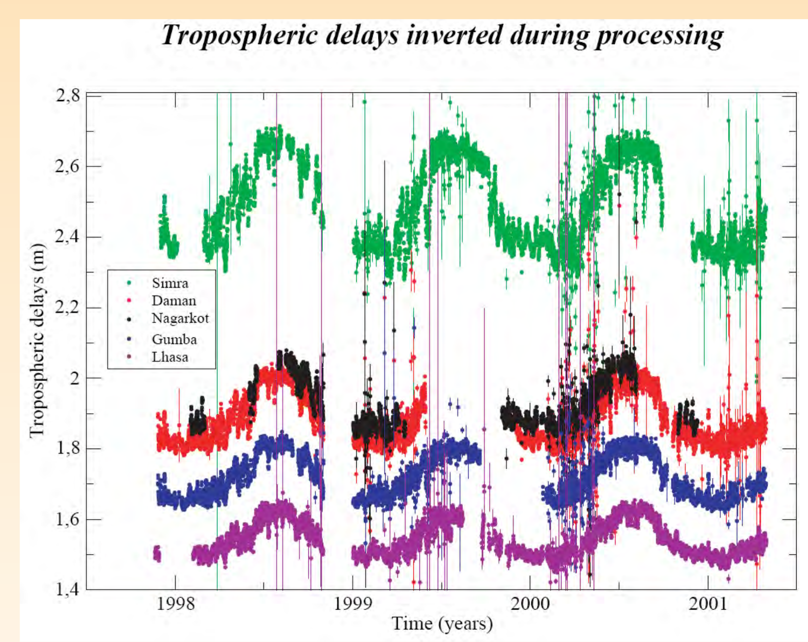

Fig. 5: Time-series of zenithal tropospheric delays at the five CGPS stations analysed in this study.

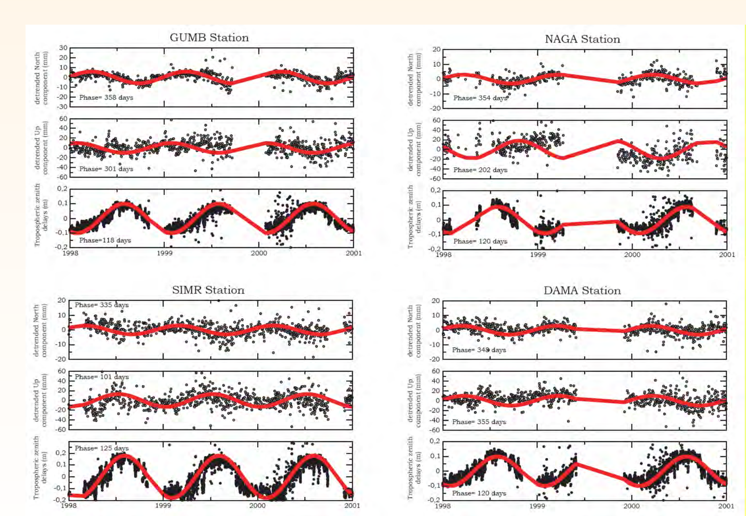

Fig. 7: Detrended northward displacements, and vertical displacements at the 4 CGPS stations SIMR, DAMA, NAGA, GUMB (black dots). Zenithal tropospheric delays inverted during the processing with BERNESE V4.2 (bottom) are shown for comparison (black dots). Red lines correspond to the best fit with a sinus function (taking into account only the annual term).

Equations

$$y(t) = a + b*t + c\cdot\sin\left(\frac{2\pi t}{T} + f_1\right) + d\cdot\sin\left(\frac{4\pi t}{T} + f_2\right) \quad (1)$$

$$\Delta r = \frac{0.002277}{\cos(z)}\left[P_b + \left(\frac{1255}{T_b}\right)\cdot e_b - B\tan^2(z)\right] + dR \quad (2)$$

$$e_b = \left(\frac{H_b}{100}\right)\cdot P_s \quad (3)$$

$$P_s = \frac{10^{\left[11-\left(\frac{2220}{T}\right)\right]}}{100} \quad (4)$$

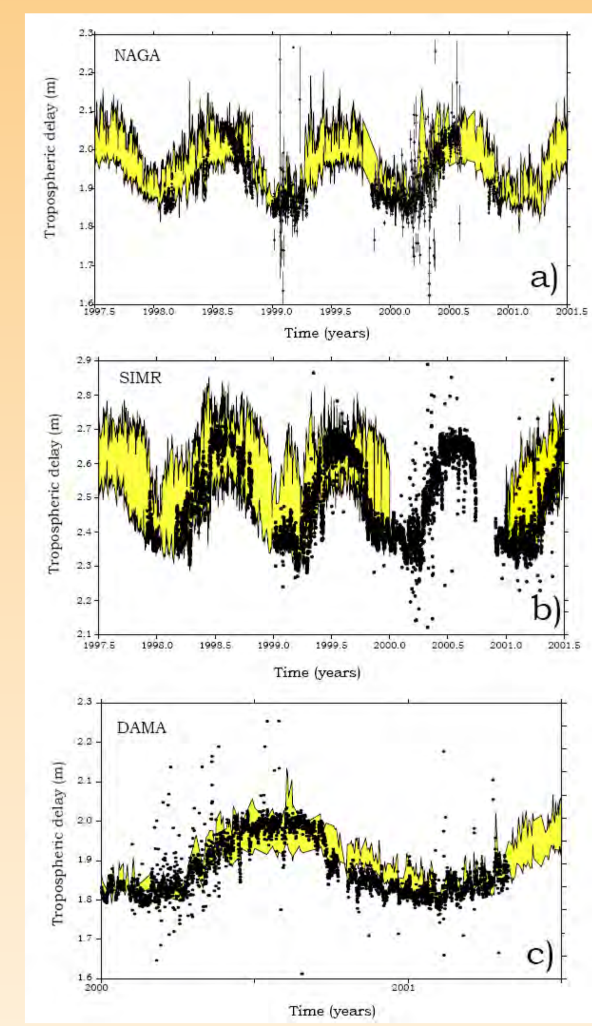

Fig. 6: Comparison of zenithal tropospheric delays determined from the processing of the GPS data (black dots) from NAGA (a), SIMR (b) and DAMA (c) and those calculated using meteorological data provided by the Nepal Department of Meteorology and Hydrology (yellow shading) and calculated from equation (2) (Saastamoinen, 1974). See Fig. 1 for location of meteorological stations.

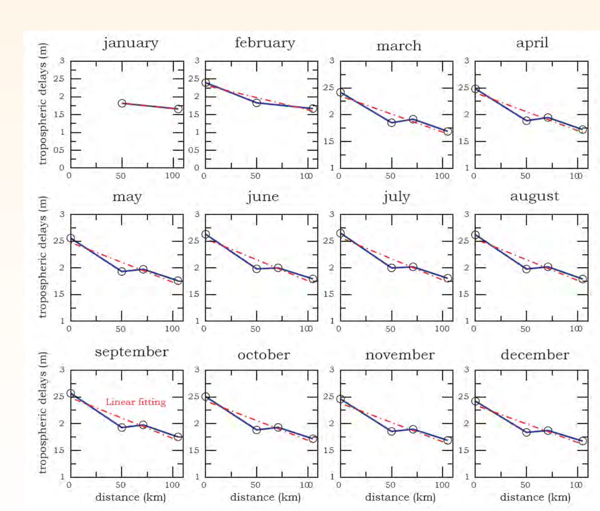

Fig. 8: Estimation of the horizontal tropospheric gradient from South to North (SIMR = 0 km; GUMB = 105 km).

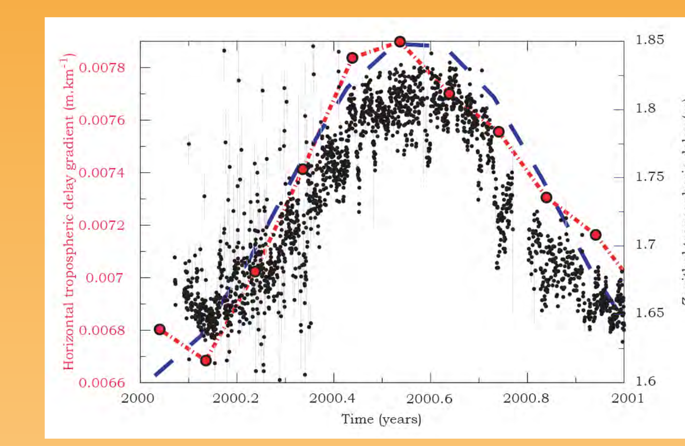

Fig. 9: Time variation of the horizontal tropospheric gradient (dashed red line). Dashed blue line corresponds to the best fit from a sinus function with a phase of 119 days. Time series of tropospheric zenithal delays computed for year 2000 (black dots).

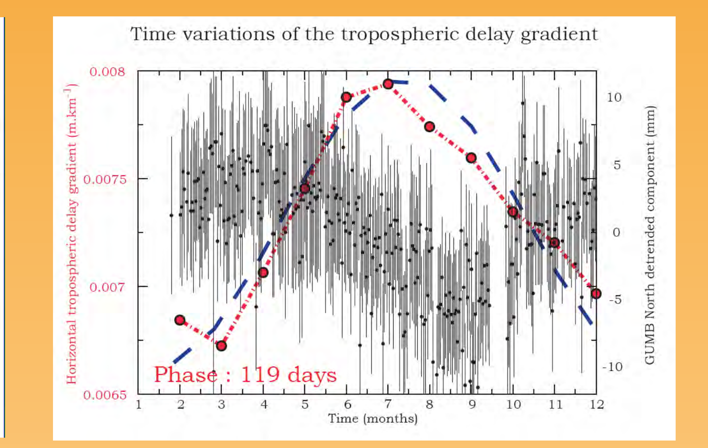

Fig. 10: Comparison between time variation of the horizontal tropospheric gradient (dashed red line) and the time series of GUMB over 2000. Dashed blue line corresponds to the best fit from a sinus function with a phase of 119 days.

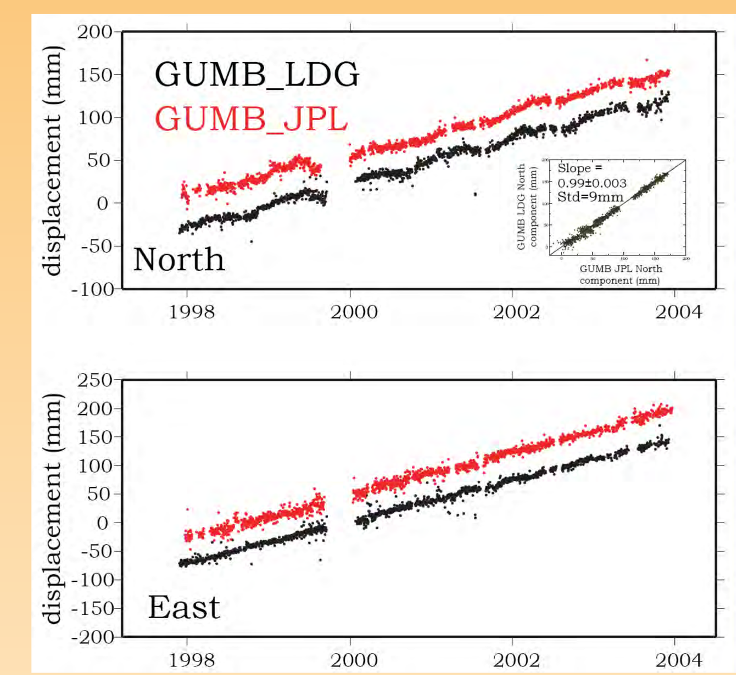

Fig. 11: Position as a function of time determined relative to ITRF2000 at the GUMB CGPS station. Black dots show positions computed with BERNESE V4.2 in which only a vertical tropospheric gradient is inverted. Red dots show positions obtained by inverting both a vertical and a horizontal tropospheric gradients computed from the Precise Point Positioning technique (Bar-Sever et al., 1998; Zumberge et al., 1997) (courtesy of P. Willis, Jet Propulsion Laboratory). Uncertainties are not shown here for clarity. The good agreement between the two time series show that the seasonal variation is due neither to a processing artefact nor to an improper account for a horizontal tropospheric gradient (inset).

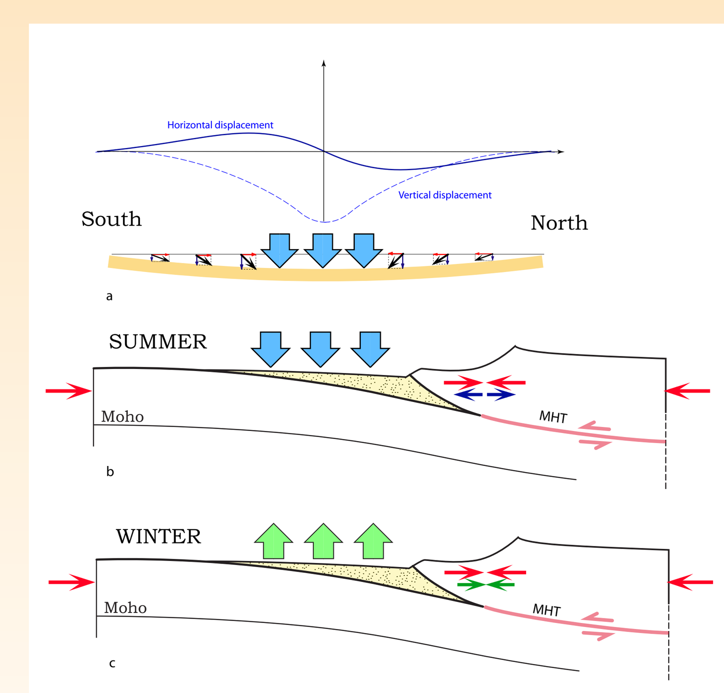

Fig. 12: Schematic diagram showing the effect of an increased water level in the Ganges basin on geodetic displacements and strain in the Himalaya. (a)Water level rise due to the summer monsoon increases the surface load (grey arrows), inducing elastic deformation of the crust. Subsidence and southward horizontal displacements occur north of the Ganges basin. Horizontal displacements south of the Ganges basin should be northward. (b) In the summer, this seasonal strain implies horizontal extension at seismogenic depth (2–15 km, blue arrows) in the Himalaya, which reduces the effect of secular horizontal compression due to interseismic strain buildup (red arrows). (c) The opposite occurs in the winter so that unloading, as water level drops, implies some horizontal compression (green arrows) that adds

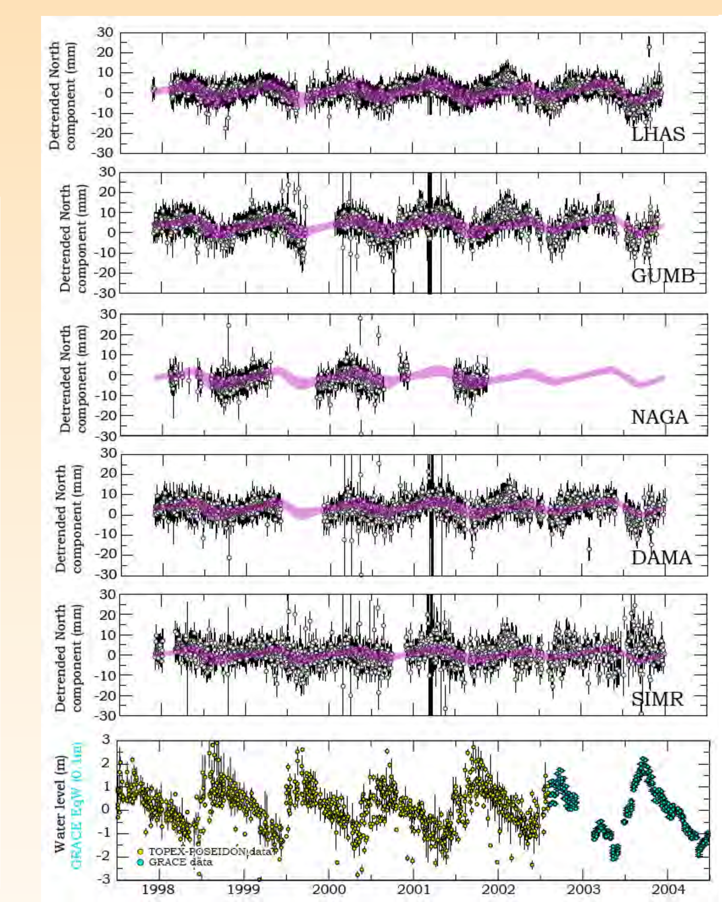

Fig. 13: Comparison of seasonal variation of geodetic displacements and water level in the Ganges basin (bottom graph). Water level variations of some major rivers in the Ganges basin measured by Topex-Poseidon (yellow dots) and equivalent water thickness derived from GRACE (blue dots). Purple shaded areas show seasonal geodetic displacements computed from the variation of surface load due to seasonal variation of water storage (2 sigma uncertainty) assuming an elastic half space with an elastic shear modulus of 40 GPa, and a Poisson coefficient of 0,25 (Bettinelli et al., submitted to EPSL).